Zn_7Metallothionein-3 and the Synaptic Vesicle Cycle: Interaction of Metallothionein-3 with the Small GTPase Rab3A†

Markus Knipp,‡ Gabriele Meloni,‡ Bernd Roschitzki,§ and Milan Vašák*

Institute of Biochemistry, University of Zürich, Winterthurerstrasse 190, CH-8057 Zürich, Switzerland

Received November 8, 2004; Revised Manuscript Received December 7, 2004

ABSTRACT: In the central nervous system, a large amount of chelatable Zn^{2+} is sequestered in presynaptic vesicles of certain glutamatergic nerve terminals. The exo-endocytotic cycle of synaptic vesicles is strictly linked to the small GTPase Rab3A. Metallothionein-3 (Zn_7MT-3) has been proposed to be involved in the intracellular trafficking of Zn^{2+} in zinc-containing neurons, but its role in this process is not understood. By using affinity precipitation and surface plasmon resonance analysis, we show that Zn_7MT-3 binds reversibly to Rab3A·GDP ($K_D = 2.6$ μM), but not to Rab3A·GTP. The binding of Zn_7MT-3 to Rab3A·GDP is specific as no binding was observed with the metal-free form of MT-3. Mutational studies of Rab3A mapped the interaction site to the effector binding site of the protein. This location is further supported by the kinetics of GDP exchange, which was found to be unaffected by binding of Zn_7MT-3 to Rab3A·GDP. The interaction of Zn_7MT-3 with Rab3A indicates that Zn_7MT-3 is not merely a cellular Zn^{2+} buffer, but actively participates in synaptic vesicle trafficking upstream of vesicle fusion.

In the mammalian brain, 10−15% of the total Zn^{2+} is localized in presynaptic vesicles of zinc-enriched neurons (ZEN),[1] which belong to a subset of glutamatergic neurons (*1*). ZEN are present in many regions of the central nervous system (CNS) and are especially abundant in hippocampus. Zn^{2+} is released from presynaptic neurons in a Ca^{2+}- and impulse-dependent fashion. The significance of Zn^{2+} in synaptic transmission is not well understood. The best-established function is that Zn^{2+} modulates the glutamate receptors onto which it is released (*2*). Zn^{2+} levels within neurons and in the extracellular space are likely to be controlled by membrane-bound Zn^{2+} transporters of the ZnT and ZIP families (*3*). The transporter that concentrates Zn^{2+} in presynaptic vesicles is ZnT3 (*4*). This has been supported by the finding that *ZnT3*$^{-/-}$ mice have no vesicular Zn^{2+} throughout the CNS (*5*). Low intracellular free Zn^{2+} concentrations are maintained by the actions of cytosolic metal-binding proteins, the most abundant of which are metallothioneins (MTs) (*6*−*8*). These proteins are present at high levels in the brain, and they reversibly bind seven Zn^{2+} ions. The Zn^{2+} ions in MTs bind with high affinity to the Cys contained in these proteins, lowering the intracellular free Zn^{2+} concentration to the pico- to nanomolar range (*9*, *10*). Besides providing a high capacity for Zn^{2+} sequestration, their function as Zn^{2+} depots providing a source of Zn^{2+} for Zn^{2+} signals and delivering Zn^{2+} to intracellular organelles has also been suggested (*11*). MT-3 represents a major component of the intracellular Zn^{2+} pool in ZEN (*12*). This protein, also termed neuronal growth inhibitory factor (GIF), occurs intra- and extracellularly and shows neuroinhibitory activity in vitro that distinguishes it from the widely expressed MT-1 and MT-2 isoforms (*13*, *14*). The importance of vesicular Zn^{2+} in kainate-induced seizure was recently studied by using *ZnT3*$^{-/-}$/*MT-3*$^{-/-}$ mice. The studies revealed that ZnT3 and MT-3 function in the same pathway (*15*).

Small GTPases act as molecular switches within cells, particularly as part of signaling pathways. They have a tightly bound guanine nucleotide, with a significant conformational difference between the GTP- and GDP-bound state. This difference in conformation state determines the activity of the proteins with respect to their interaction with effectors. Small Rab GTPases couple signal transduction networks to the membrane trafficking machinery (*16*). The small GTPase Rab3A and MT-3 have been found colocalized in hippocampal neurons (*17*, *18*), and their interaction has been implicated via yeast two-hybrid system studies (*19*). Of the many Rab family members involved in the vesicular targeting and docking process, Rab3A is involved in Ca^{2+}-dependent exocytosis, particularly in the release of neurotransmitter from nerve terminals (*20*).

By applying affinity precipitation and surface plasmon resonance (SPR), we demonstrate that Zn_7MT-3 binds reversibly to Rab3A·GDP, but not to Rab3A·GTP. Further-

† This work was supported by Swiss National Science Foundation Grant 3100A0-100246/1, by the "Forschungskommission und Nachwuchsförderungskommission der Universität Zürich" (to M.K.), the "EMDO Stiftung" (to B.R.), and the "Jubiläumsspende der Universität Zürich".

* To whom correspondence should be addressed: Institute of Biochemistry, University of Zürich, Winterthurerstrasse 190, CH-8057 Zürich, Switzerland. Telephone: +41-1-6355552. Fax: +41-1-6355905. E-mail: mvasak@bioc.unizh.ch.

‡ These authors contributed equally to this work.

§ Present address: Functional Genomics Center Zürich (FGCZ), Winterthurerstrasse 190, CH-8057 Zürich, Switzerland.

[1] Abbreviations: CNS, central nervous system; DTT, 1,4-dithio-D,L-threitol; GDI, GDP dissociation inhibitor; GppNHp, guanosine 5′-(β,γ-imido)triphosphate; GSH, glutathione; mantGDP, 2′(3′)-bis-*O*-(*N*-methylanthraniloyl)guanosine 5′-diphosphate; HEPES, 4-(2-hydroxyethyl)piperazine-1-ethanesulfonic acid; MT, metallothionein; RabCDR, Rab complementarity-determining region; RU, response units; SPR, surface plasmon resonance; ZEN, zinc-enriched neurons; ZIP, Zrt- and Irt-like proteins; ZnT, zinc transporter.

10.1021/bi047636d CCC: $30.25
Published on Web 02/08/2005

more, the binding is specific as no interaction was observed with the metal-free form of MT-3. We show that the interaction between Zn_7MT-3 and Rab3A does not affect the GDP exchange rate. Additionally, we show that Zn_7MT-3 binds to the effector binding site of Rab3A. These findings identify Zn_7MT-3 as a protein involved in synaptic vesicle trafficking upstream of vesicle fusion.

EXPERIMENTAL PROCEDURES

Materials. Media for protein expression were purchased from BD (Becton, Dickinson and Co., Sparks, MD). Glutathione Sepharose Fast Flow 4 was purchased from Amersham Biosciences. GDP (≥95%) and guanosine 5′-(β,γ-imido)triphosphate (GppNHp, 93%) were purchased from Sigma. GTP (80%) was obtained from Roche, and 2′(3′)-bis-*O*-(*N*-methylanthraniloyl)guanosine 5′-diphosphate (mantGDP) was obtained from Molecular Probes. All reagents for SPR experiments were purchased directly from the instrument manufacturer (Biacore AB, Uppsala, Sweden). All other standard reagents were of the highest purity available from common commercial sources.

Construction of the GST−Rab3A(2−186) Expression Vector. The expression plasmid pET3c-Rab3a was generously provided by F. Darchen (*21*). The cDNA of the Rab3A-(2−186) deletion mutant was amplified by PCR from pET3c-Rab3a using the following primers: 5′-TAG GAT CCG CAT CTG CCA CAG-3′ and 5′-GTC ATC TGC GAG AAG TGA ATT CAT-3′. The product was subcloned into the pGEX-2T vector (Amersham Biosciences) using *Bam*HI and *Eco*RI as restriction sites. The correctness of the construct was verified by matrix-assisted laser desorption ionization time-of-flight mass spectrometry (MALDI-TOF MS) upon protein expression (calculated for [GST−Rab3A(2−186) + H^+], 47 638 Da; observed, 47 672 Da).

Protein Expression and Purification. MT-3 was expressed in *Escherichia coli* and purified as described previously (*22*, *23*). Fully Zn^{2+}-loaded MT-3 was prepared by reconstitution (*24*). Metal:protein ratios were determined by measuring the metal content by flame atomic absorption spectroscopy (SpectrAA-110, Varian Inc.) (*22*) and that of the protein spectrophotometrically in 0.1 M HCl (ϵ_{220} = 53 000 M^{-1} cm^{-1}) (*25*). In all cases, a metal:protein ratio of 7.0 ± 0.3 was obtained.

The expression plasmid pGEX-rab3A for full-length GST−Rab3A was a gift of K. Kirk (*26*). Full-length Rab3A and Rab3A(2−186) were expressed in *E. coli* as GST fusion proteins and purified as previously described (*26*). Concentrations of these proteins were determined with the Bio-Rad *DC* protein assay using bovine serum albumin as a standard. GST−Rab3A and GST−Rab3A(2−186) were tested for GTPase activity by the determination of the amount of P_i released as described previously (*27*).

Carboxyamidomethylation of MT-3. The Cys residues of MT-3 were modified by carboxyamidomethylation with iodoacetamide. For the preparation of carboxyamidomethylated MT-3, the metal-free protein was generated (*24*). Subsequently, metal-free MT-3 (apoMT-3) was incubated in the dark in 500 mM Tris-HCl, 6 M guanidine·HCl, 5 mM EDTA, and 10 mM DTT (pH 8.6) for 45 min. A 25-fold excess of iodoacetamide over DTT was added to this mixture (*28*). The excess of iodoacetamide was removed through a Sephadex G-25 superfine size exclusion column (Amersham Biosciences). The correctness of the modification was verified by amino acid analysis (Applied Biosystems Inc. 420A/H amino acid analyzer) and by the determination of the free Cys content with 2,2′-dithiopyridine (<1 molar equiv).

Affinity Precipitation. Because GTP will be hydrolyzed when bound to Rab3A, affinity precipitations were performed with the stable analogue GppNHp instead. To prepare GDP or GppNHp-loaded GST−Rab3A, a 5 μM solution of the protein was first incubated for 3 h at 30 °C in 10 mM HEPES-NaOH, 150 mM KCl, 1 mM DTT, and 1 mM EDTA (pH 7.4), which contained either 1 mM GDP or 1 mM GppNHp. Subsequently, 5 mM $MgCl_2$ was added and the incubation continued for 30 min; 100 μL of Glutathione Sepharose 4 Fast Flow beads were loaded by adding 500 μL of 5 μM GST−Rab3A·GDP, GST−Rab3A·GppNHp, or, as a control, GST alone. After incubation for 20 h at 4 °C, 1 mL of 50 μM Zn_7MT-3 was added and the incubation continued for 2 h at room temperature. Then the resin was washed three times with 750 μL of 10 mM HEPES-NaOH, 50 mM KCl, 5 mM $MgCl_2$, and 1 mM DTT (pH 7.4). Upon addition of 50 μL of 50 mM Tris-HCl and 1% (w/v) SDS (pH 8.0), samples were heated for 10 min at 95 °C. For immunodetection of MT-3, Cys residues were modified with monobromobimane (30 μL samples). The samples were analyzed by SDS−PAGE (15%) and blotted onto a nitrocellulose membrane.[2] The Western blot was developed using anti-hMT-3α (*29*).

Surface Plasmon Resonance (SPR) Binding Studies. SPR experiments were performed using a Biacore 3000 instrument (Biacore AB) and a caboxymethylated CM5 sensor chip to which an anti-GST antibody was covalently coupled using reagents and protocols supplied by the manufacturer. GST and the GST fusion proteins Rab3A and Rab3A(2−186) were captured to a surface density between 1000 and 2000 response units (RU) through injection of 1 μM samples at a flow rate of 5 μL/min at 30 °C. GST−Rab3A and GST−Rab3A(2−186) were loaded with either GDP or GppNHp as described for affinity precipitation. The full nucleotide loading of the proteins after capturing was achieved by injecting 50 μL of 2 mM GDP or GppNHp. Prior to being used, Zn_7MT-3 was passed over a Superdex 75 HR 10/30 size-exclusion column (Amersham Biosciences) in 10 mM HEPES-NaOH, 50 mM KCl, and 5 mM $MgCl_2$ (pH 7.4). For SPR binding experiments, all captured proteins were brought into degassed flow buffer [10 mM HEPES-NaOH, 50 mM KCl, 5 mM $MgCl_2$, and 0.005% (v/v) Tween 20 (pH 7.4)] prior to analyte injection. In SPR experiments, no DTT was added to the buffers to avoid the reduction and following inactivation of antibodies immobilized on the chip surface. Tandem flow cells were utilized; one was loaded with GST−Rab3A or GST−Rab3A(2−186) (sample channel), and the other was loaded with GST (reference channel). The interaction between various forms of GST−Rab3A and Zn_7MT-3 was studied using a flow rate of 20 μL/min. In each set of experiments, increasing Zn_7MT-3 concentrations of up to 103 μM were injected (see figure captions). The dissociation was initiated by stopping the injection of protein while the flow of running buffer was maintained. The

[2] The method will be published elsewhere.

decrease in the magnitude of the SPR signal in the dissociation phase with time was monitored until the initial level of RU was reached. After each set of injections, the anti-GST antibody surface was regenerated with 10 mM Gly-HCl (pH 2.2). Binding data were evaluated using steady-state analysis, plotting the plateau of the SPR signal versus the analyte concentration. Data were fitted by nonlinear regression analysis employing BIAevaluation 3.0 (Biacore AB). The dissociation constant K_D was obtained from a fit to the hyperbolic equation

$$R_{eq} = R_{max}[Zn_7MT\text{-}3]/(K_D + [Zn_7MT\text{-}3])$$

Independently, from the change in SPR signal with time (dRU/d*t*) were estimated the association and dissociation rate constants. The association and dissociation phases were fitted to rate equations provided in BIAevaluation 3.0 for a Langmuir 1:1 binding model.

Nucleotide Release Assays. GST−Rab3A was loaded with the fluorescent GDP analogue mantGDP by incubation for 3.5 h at 30 °C in 10 mM HEPES-NaOH, 150 mM KCl, and 1 mM EDTA (pH 7.4) containing a 10-fold excess of mantGDP over GST−Rab3A. The reaction was terminated by the addition of 5 mM $MgCl_2$. Unbound mantGDP was removed on a 5 mL HiTrap desalting column (Amersham Biosciences). For nucleotide release assays, GST−Rab3A·mantGDP was diluted to 77 nM in 10 mM HEPES-NaOH, 100 mM KCl, 1 mM DTT, and 0.5 mM $MgCl_2$ (pH 7.4) in a quartz cuvette. The dissociation of mantGDP in the absence or presence of 27 μM Zn_7MT-3 was initiated by the addition of 1 mM GDP. Upon excitation at 360 nm, the fluorescence emission of mantGDP was monitored at 440 nm on a SPEX fluorolog spectrofluormeter using bandwidths of 9.0 nm for excitation and 4.5 nm for emission. The internal light shutter of the instrument was employed to prevent photodecay of mantGDP. Data points were collected every 60 s with an integration time of 1 s. The dissociation rate constants k_{off} and k_{obs} were obtained from two independent measurements employing Origin version 7.5 (OriginLab Corp., Northampton, MA) through fitting to the equation

$$I(t) = (I_0 - I_\infty)\exp(-k_{off}t) + I_\infty$$

RESULTS

Affinity Precipitation of Zn_7MT-3 and Rab3A. To explore a protein−protein interaction between MT-3 and Rab3A, affinity precipitation experiments were performed first. Therefore, GST−Rab3A was loaded with either GDP or the nonhydrolyzable GTP analogue GppNHp and then immobilized on Glutathione Sepharose beads. This step was followed by incubation with Zn_7MT-3. To prevent the formation of disulfides between Rab3A and Zn_7MT-3, 1 mM DTT was added. Under these conditions, no Zn^{2+} was extracted from Zn_7MT-3. After being extensively washed, Zn_7MT-3 bound to the beads was detected with polyclonal antibodies against the α-domain of MT-3 [anti-hMT-3α (*29*)]. Similar experiments employing GST and Zn_7MT-3 were used as controls. As shown in Figure 1, Zn_7MT-3 was only detected together with Rab3A·GDP, but not with Rab3A·GppNHp, i.e., Rab3A·GTP.

Surface Plasmon Resonance (SPR) Analysis of the Interaction of Zn_7MT-3 with GST−Rab3A. To further investigate

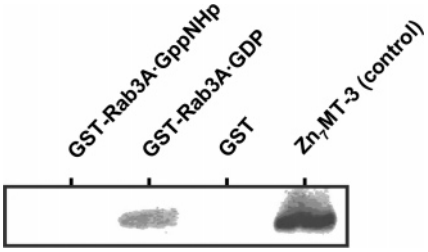

FIGURE 1: Affinity precipitation of GST−Rab3A with Zn_7MT-3. GST−Rab3A·GppNHp, GST−Rab3A·GDP, or GST was bound to Glutathione Sepharose beads and incubated with 50 μM Zn_7-MT-3 in the presence of 1 mM DTT. After being extensively washed, samples were analyzed by Western blot using anti-MT-3α antibodies (*29*).

the interaction of Rab3A and Zn_7MT-3, we have carried out SPR experiments. SPR is a powerful tool for real time measurements of direct protein−protein interactions that does not require labeling of the proteins. In contrast, protein−protein interactions detected by a yeast two-hybrid system or pull-down method may sometimes reflect nonspecific binding. The amplitude of the SPR signal is proportional to the mass of the bound analyte. Because of the rather low molecular mass of Zn_7MT-3 (~7 kDa), only a small SPR signal was expected. In our experiments, we used tandem flow cells where in one cell (sample channel) GST−Rab3A and in the other (reference channel) only GST was captured. Care was taken to capture similar quantities of these proteins based on response units (RU). This setup allowed a direct subtraction of SPR signals in both cells. When Zn_7MT-3 was injected at concentrations in the low micromolar range, a concentration-dependent reversible binding to the GST−Rab3A·GDP-bound form was observed (Figure 2A). As judged by the amplitude of the SPR signal, weak reversible binding also occurred when Zn_7MT-3 was injected over a GST−Rab3A·GppNHp-loaded surface (Figure 2B). Major contributions to this signal can be ascribed to incomplete exchange of GDP for GppNHp in the sample preparation and to the presence of residual GDP in the GppNHp form (as indicated by the manufacturer). In these SPR studies, each set of experiments was performed five times. The quantity of Zn_7MT-3 bound at equilibrium (R_{eq}) to GST−Rab3A·GDP saturates at low micromolar concentrations (Figure 2A). The signals observed show typical association and dissociation characteristics, and from these data, a steady-state plot was obtained (Figure 2C). The data are well fit by a simple Langmuir binding isotherm, yielding a dissociation constant K_D of 2.6 ± 1.5 μM. Association and dissociation rate constants were obtained from the signal courses of the association and dissociation phases, respectively, assuming Langmuir 1:1 binding. An association rate constant k_{on} of $\approx 10^4$ M^{-1} s^{-1} and a dissociation rate constant k_{off} of $\approx 10^{-2}$ s^{-1} were estimated.

The three-dimensional structure of Zn_7MT-3 is mainly dictated by Zn^{2+} binding (*7*). To show that a well-defined MT-3 structure is required for the Zn_7MT-3·Rab3A·GDP interaction, the binding of metal-free MT-3 (apoMT-3) was also examined. To protect the 20 Cys residues of apoMT-3 from oxidation, prior to injection all Cys residues were carboxyamidomethylated. The SPR experiments revealed no interaction with GST−Rab3A·GDP up to 10 μM apoMT-3 (data not shown). Overall, these results indicate that the Zn_7-

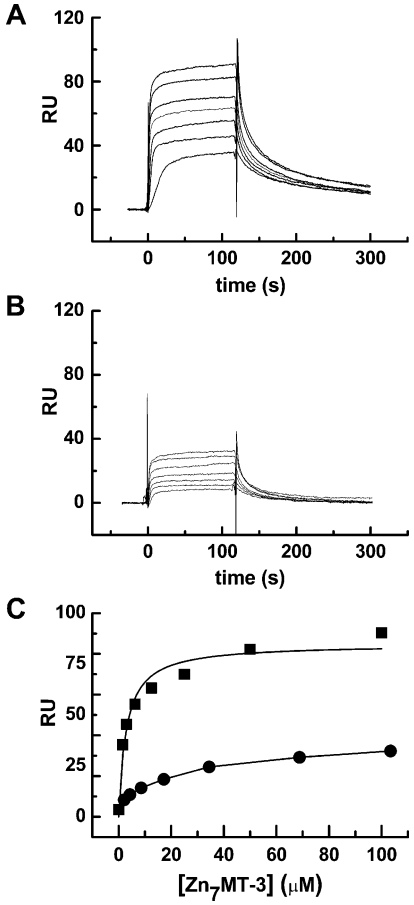

FIGURE 2: Surface plasmon resonance analysis of the interaction of GST−Rab3A with Zn_7MT-3. (A) Representative SPR sensograms following injection of 1.56, 3.1, 6.3, 12.5, 25, 50, and 100 μM Zn_7MT-3 into tandem flow cells loaded with GST−Rab3A·GDP (sample channel) and GST (reference channel) with on-line signal subtraction. (B) As in panel A, but with GST−Rab3A·GppNHp loaded (sample channel) and 2.1, 4.3, 8.6, 17.2, 34, 69, and 103 μM of Zn_7MT-3 injected. (C) Representative concentration dependence plots of the equilibrium SPR signal (R_{eq}) for binding of Zn_7MT-3 to GST−Rab3A loaded with (■) GDP or (●) GppNHp.

MT-3 interaction occurs with the GST−Rab3A·GDP form and that this interaction is specific.

Mapping the Zn_7MT-3·Rab3A Interaction Site. The structure of Rab3A is characterized by a long unstructured C-terminal tail (residues 190−220). This hypervariable extension is required for prenylation and targeting to specific intracellular membranes, but it is not essential for nucleotide binding or hydrolysis. This extension has been removed in the crystal structure of Rab3A(15−186) without affecting its GTPase activity (*30*). Therefore, the deletion mutant GST−Rab3A(2−186) was generated, and SPR binding studies were performed using GST−Rab3A(2−186)·GDP and Zn_7MT-3 as described above for the wild-type protein. In Figure 3, the resulting steady-state plot of GST−Rab3A-(2−186) is compared to that of the wild-type protein. The former data are well fit by a simple Langmuir binding isotherm, yielding a dissociation constant K_D of 12 ± 2 μM. The lower affinity for Rab3A(2−186) compared to the wild-type protein suggests that the C-terminal region of Rab3A is important for the binding of Zn_7MT-3.

Effect of Binding of Zn_7MT-3 to Rab3A·GDP on Nucleotide Dissociation. To examine the effect of the Zn_7MT-3·Rab3A·GDP interaction on the structure of Rab3A, we have

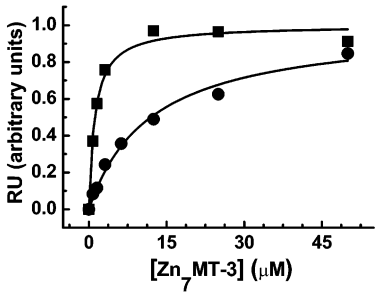

FIGURE 3: Effect of C-terminal Rab3A truncation on Zn_7MT-3 binding. Representative concentration dependence plots of the equilibrium SPR signal (R_{eq}) for binding of Zn_7MT-3 to (■) GST−Rab3A·GDP or (●) GST−Rab3A(2−186)·GDP. Data were obtained with a set of increasing Zn_7MT-3 concentrations (between 0.78 and 50 μM) and were normalized to the maximum signal to place both sets of data on the same scale.

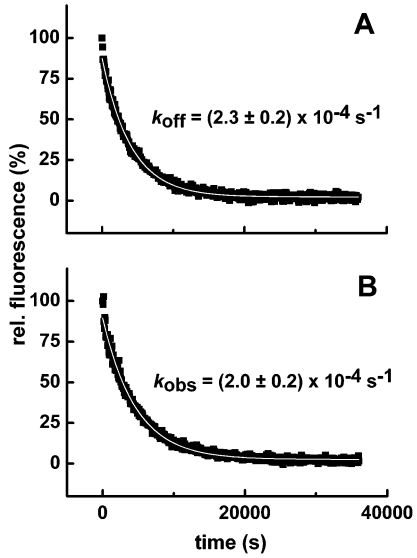

FIGURE 4: Effect of Zn_7MT-3 binding on the kinetics of nucleotide release from GST−Rab3A. Fluorescence time course for the dissociation of mantGDP from GST−Rab3A (77 nM) in the absence (A) or presence (B) of 27 μM Zn_7MT-3. The fluorescence decay was monitored upon the addition of 1 mM GDP (excitation at 360 nm and emission at 440 nm). Curves were fitted with a first-order kinetic model, yielding the indicated dissociation rate constants.

studied the GDP exchange rates in the presence and absence of Zn_7MT-3. Therefore, GST−Rab3A was first loaded with the fluorescent analogue of GDP, mantGDP. When mantGDP was excited at 360 nm, its dissociation was followed upon the addition of excess GDP through the decreasing fluorescence of mantGDP emission at 440 nm (Figure 4). Assuming a single-exponential decay, the release process in the presence of Zn_7MT-3 [Figure 4B; $k_{obs} = (2.0 \pm 0.2) \times 10^{-4}$ s^{-1}] was as fast as in its absence [Figure 4A; $k_{off} = (2.3 \pm 0.2) \times 10^{-4}$ s^{-1}]. In this case, the nucleotide release from the binary complex (Rab3A·GDP) is designated as k_{off} and that from the ternary complex (Zn_7MT-3·Rab3A·GDP) as k_{obs}. Since the kinetics of nucleotide release were found to be unaffected by the formation of the ternary complex and since its formation was much faster than nucleotide release, k_{obs} is a direct measure of k_{off}.

DISCUSSION

In the CNS, large amounts of Zn^{2+} accumulate in presynaptic vesicles of ZEN by a mechanism that requires

zinc transporter ZnT3 at the vesicular membrane (*4*, *15*, *17*). In response to stimulation, Zn^{2+} is released into the synaptic cleft through exocytosis. The small GTPase Rab3A is involved in vesicular trafficking processes and is highly expressed in neurons where it associates with the membranes of synaptic neurotransmitter vesicles (*2*, *16*, *31*). MT-3 represents a major component of the intracellular Zn^{2+} pool in ZEN. This protein binds typically seven Zn^{2+} ions into two metal−thiolate clusters. In contrast to the MT-1 and MT-2 isoforms, both MT-3 clusters assemble with metal ions in a noncooperative manner (*25*, *32*, *33*). More recent studies established the presence of one redox labile metal site in the protein structure (*23*). In addition, MT-3 containing fewer than seven Zn^{2+} ions is stable. Apart from these unusual metal binding properties, MT-3 also exhibits an unprecedented conformational flexibility and cluster dynamics recognized to be important for a protein−protein interaction (*34*). These properties together with the abundance of Zn_7-MT-3 in ZEN suggest that it plays an important role in handling of Zn^{2+} in these cells. This hypothesis is supported by the work on the role of vesicular Zn^{2+} in kainate-induced seizure revealing that ZnT3 and MT-3 function in the same pathway (*15*) and by immunohistochemical studies of the rat brain which localized MT-3 in association with synaptic vesicles and postsynaptic densities (*35*). In the study reported here, evidence for the interaction of Zn_7MT-3 with Rab3A is presented.

Initially, we have studied the protein−protein interaction by affinity precipitation. The obtained results revealed an interaction of Zn_7MT-3 with Rab3A·GDP but not with Rab3A·GTP (Rab3A·GppNHp). Our SPR experiments established that the interaction of Zn_7MT-3 with Rab3A·GDP is specific as no binding was observed with the predominantly unstructured apoMT-3 form. The determined dissociation constant for the Zn_7MT-3·Rab3A·GDP complex equaled 2.6 μM. This value is comparable to those of other well-established Rab−protein interactions such as Rab3A·Rim1 ($K_D = 1-2\ \mu$M) (*36*) or Rab5C·EEA1 ($K_D = 3.3\ \mu$M) (*37*). In this context, it should be mentioned that the cytosolic amount of MT-3 is relatively large (*38*), which would shift the equilibrium of the interaction to the complex site. To gain insight into the Zn_7MT-3·Rab3A·GDP interaction at the molecular level, a deletion mutant of Rab3A lacking the C-terminal tail (residues 187−220) was generated. The corresponding SPR experiments showed that Zn_7MT-3 has approximately 5 times weaker affinity for Rab3A(2−186) than that obtained for the wild-type protein. This suggests that the C-terminal region of Rab3A is important for the Zn_7MT-3·Rab3A·GDP interaction.

Rab3A interacts with many effector proteins in its GTP-bound form. The binding or release of the effector to or from Rab3A is mediated through two switch regions. They exhibit a significant conformational difference between the GTP- and GDP-bound state and are thus responsible for the selectivity of the effector binding. In addition, the effector binding involves three Rab complementarity-determining regions (RabCDRs). Figure 5A shows the crystal structure of Rab3A(16−192) (*39*) with the switch regions (yellow) and the RabCDRs (blue) indicated. Besides the involvement of the C-terminal region (RabCDR3) of Rab3A in Zn_7MT-3 binding, the protein−protein interaction also distinguishes between the GDP- and GTP-bound form of Rab3A. There-

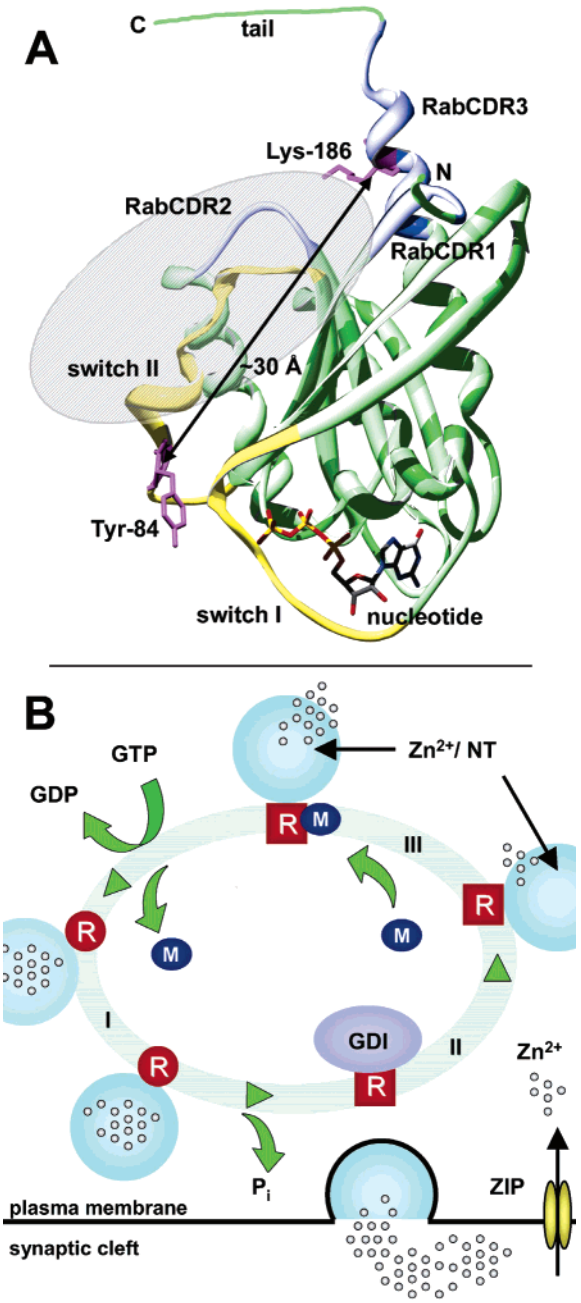

FIGURE 5: Model for the interaction of Zn_7MT-3 with Rab3A in the synaptic vesicle cycle. (A) Proposed binding surface for Zn_7-MT-3 on Rab3A. The crystal structure of Rab3A(16−192) (PDB entry 1ZBD) is shown in a complex with GppNHp (*39*). The three RabCDR sites are colored blue and the two switch regions yellow. The distance between RabCDR3 (Lys-186, purple) and the switch region II (Tyr-84, purple) spans approximately 30 Å (black arrow). On the basis of the data presented in this study, Zn_7MT-3 (overall dimensions of $a \approx 40$ Å and $b \approx c \approx 20$ Å; represented as a gray oval) likely binds in the cleft formed by the RabCDRs and the switch regions opposite from the nucleotide-binding site. This panel was generated using Swiss-PDB Viewer version 3.7 (*50*). (B) Putative simplified scheme of the involvement of MT-3 in the exo-endocytotic cycle of synaptic vesicles: R in circle, Rab3A·GTP; R in square, Rab3A·GDP; M, MT-3; NT, neurotransmitter. For simplification, the exo-endocytotic cycle was divided into phases I−III according to the accessibility of MT-3 for interaction with Rab3A. In phase I, MT-3 does not bind to the Rab3A·GTP complex. In phase II, upon hydrolysis of GTP, Rab3A·GDP is complexed with GDI which makes the interaction surface inaccessible for MT-3. In phase III, Rab3A·GDP is bound to the vesicular membrane and the binding interface for MT-3 is accessible (for the complete synaptic vesicle cycle, see ref *18*).

fore, Zn_7MT-3 must also interact with at least one of the switch regions. The distance between Lys-186 in RabCDR3 and the switch region II spans ~30 Å (see Figure 5A). The three-dimensional structure of MT-3 has not yet been fully elucidated (*40*), but by analogy to the structure of MT-2 (PDB entry 4MT2), this distance corresponds well to the size of the MT-3 molecule. The nucleotide-binding site in this model is located at the opposite end. This location is in agreement with our studies of the mantGDP exchange rates, which were found to be unaffected by the binding of Zn_7-MT-3.

Interestingly, Rab3A, ZnT3, and MT-3 are colocalized at the vesicular membrane in CA1 and CA3 neurons of hippocampus, in which Zn^{2+} ions accumulate in presynaptic vesicles (*17*, *18*). The cycling of Rab3A between the GTP- and GDP-bound state is strictly linked to the exo-endocytotic cycle of synaptic vesicles (*18*, *41*). Although we have demonstrated the physical interaction of Zn_7MT-3 with Rab3A·GDP, the involvement of a number of other proteins in synaptic vesicle cycling is well established (*18*). In Figure 5B, a putative simplified scheme of the involvement of Zn_7-MT-3 in this process consistent with our data and literature reports is presented. After fusion of the vesicle with the synaptic membrane, the membrane-bound Rab3A hydrolyzes GTP and Rab3A·GDP dissociates from the vesicular membrane by the action of the GDP dissociation inhibitor (GDI). Rab3A·GDP is then delivered to synaptic vesicles where GDI is released concomitantly with Rab3A·GDP binding (*42*). At this step of the cycle, Zn_7MT-3 may bind to Rab3A·GDP. The binding of Zn_7MT-3 to GDI·Rab3A·GDP in the cytosol is unlikely as in the crystal structure of the complex between the Rab homologue YPT1·GDP from yeast and GDI both the C-terminal region and the switch II region are inaccessible (*43*). However, the function of Zn_7MT-3 bound to Rab3A·GDP at the vesicular membrane is not clear. We hypothesize that it may function as an effector, Zn^{2+} sensor, or chaperone delivering Zn^{2+} to the vesicular membrane where it is compartmentalized by ZnT3. Effector proteins upon their binding to Rab proteins can recruit other binding partners forming multiprotein complexes through which various functions are mediated. The term effector has been used mainly for proteins recruited by the GTP-bound form of Rab proteins. However, examples of binding partners for the GDP-bound form are also known (*20*). Because of the high metal binding capacity of Zn_7MT-3, its biological function is more likely related to metal handling. As a Zn^{2+} sensor, metal-free or partially metal-loaded MT-3 may be involved in sensing synaptic Zn^{2+} concentrations. The binding of fully metal-loaded Zn_7MT-3 to Rab3A·GDP may affect the rate of exocytosis of synaptic vesicles. Another attractive possibility is that MT-3 may facilitate recycling of Zn^{2+} to synaptic vesicles. Such a chaperone function would be particularly important in a rapid delivery of Zn^{2+} taken up from the synaptic cleft. The binding of Zn_7MT-3 to the Rab3A·GDP form may reflect the specific point of the synaptic vesicle cycle where such a Zn^{2+} delivery occurs. We have noted that in other cell types that store large amounts of chelatable Zn^{2+}, the presence of Rab3A and MT-3 has also been reported. These include insulin-secreting pancreatic β-cells (*44*−*46*) and testis (*47*−*49*). The results reported here, indicating that Zn_7MT-3 is involved in the physical interaction with the small GTPase Rab3A, provide the basis for a better understanding of its role in various Zn^{2+}-rich cell types.

ACKNOWLEDGMENT

We thank Dr. K. L. Kirk (University of Alabama, Tuscaloosa, AL) and Dr. F. Darchen (CNRS, Paris, France) for the generous gift of plasmids pGEX-rab3A and pET3c-Rab3a, respectively.

REFERENCES

1. Frederickson, C. J. (1989) Neurobiology of zinc and zinc-containing neurons, *Int. Rev. Neurobiol. 31*, 145−238.
2. Frederickson, C. J., and Bush, A. I. (2001) Synaptically released zinc: Physiological functions and pathological effects, *BioMetals 14*, 353−366.
3. Liuzzi, J. P., and Cousins, R. J. (2004) Mammalian zinc transporters, *Annu. Rev. Nutr. 24*, 151−172.
4. Palmiter, R. D., Cole, T. B., Quaife, C. J., and Findley, S. D. (1996) ZnT-3, a putative transporter of zinc into synaptic vesicles, *Proc. Natl. Acad. Sci. U.S.A. 93*, 14934−14939.
5. Cole, T. B., Wenzel, H. J., Kafer, K. E., Schwartzkroin, P. A., and Palmiter, R. D. (1999) Elimination of zinc from synaptic vesicles in the intact mouse brain by disruption of the ZnT3 gene, *Proc. Natl. Acad. Sci. U.S.A. 96*, 1716−1721.
6. Palmiter, R. D. (1998) The elusive function of metallothioneins, *Proc. Natl. Acad. Sci. U.S.A. 95*, 8428−8430.
7. Vašák, M., and Hasler, D. W. (2000) Metallothioneins: New functional and structural insights, *Curr. Opin. Chem. Biol. 4*, 177−183.
8. Hidalgo, J., Aschner, M., Zatta, P., and Vašák, M. (2001) Roles of the metallothionein family of proteins in the central nervous system, *Brain Res. Bull. 55*, 133−145.
9. Outten, C. E., and O'Halloran, T. V. (2001) Femtomolar sensitivity of metalloregulatory proteins controlling zinc homeostasis, *Science 292*, 2488−2492.
10. Finney, L. A., and O'Halloran, T. V. (2003) Transition metal speciation in the cell: Insights from the chemistry of metal ion receptors, *Science 300*, 931−936.
11. Vallee, B. L., and Falchuk, K. H. (1993) The biochemical basis of zinc physiology, *Physiol. Rev. 73*, 79−118.
12. Erickson, J. C., Hollopeter, G., Thomas, S. A., Froelick, G. J., and Palmiter, R. D. (1997) Disruption of the metallothionein-III gene in mice: Analysis of brain zinc, behavior, and neuron vulnerability to metals, aging, and seizures, *J. Neurosci. 17*, 1271−1281.
13. Uchida, Y., Takio, K., Titani, K., Ihara, Y., and Tomonaga, M. (1991) The growth inhibitory factor that is deficient in the Alzheimer's disease brain is a 68 amino acid metallothionein-like protein, *Neuron 7*, 337−347.
14. Uchida, Y., Gomi, F., Masumizu, T., and Miura, Y. (2002) Growth inhibitory factor prevents neurite extension and death of cortical neurons caused by high oxygen exposure through hydroxyl radical scavenging, *J. Biol. Chem. 277*, 32353−32359.
15. Cole, T. B., Robbins, C. A., Wenzel, H. J., Schwartzkroin, P. A., and Palmiter, R. D. (2000) Seizures and neuronal damage in mice lacking vesicular zinc, *Epilepsy Res. 39*, 153−169.
16. Takai, Y., Sasaki, T., and Matozaki, T. (2001) Small GTP-binding proteins, *Physiol. Rev. 81*, 153−208.
17. Lee, J.-Y., Kim, J.-H., Palmiter, R. D., and Koh, J.-Y. (2003) Zinc released from metallothionein-III may contribute to hippocampal CA1 and thalamic neuronal death following acute brain injury, *Exp. Neurol. 184*, 337−347.
18. Südhof, T. C. (2004) The synaptic vesicle cycle, *Annu. Rev. Neurosci. 27*, 509−547.
19. Kang, Q. H., Chen, Q. L., Ren, H. W., and Ru, B. G. (2001) Growth inhibitory factor (GIF) directly interacts with G-protein Rab3a, *Prog. Biochem. Biophys. 28*, 880−884.
20. Takai, Y., Sasaki, T., Shirataki, H., and Nakanishi, H. (1996) Rab3A small GTP-binding protein in Ca^{2+}-dependent exocytosis, *Genes Cells 1*, 615−632.
21. Zahraoui, A., Touchot, N., Chardin, P., and Tavitian, A. (1989) The human *Rab* genes encode a family of GTP-binding proteins related to yeast YPT1 and SEC4 products involved in secretion, *J. Biol. Chem. 264*, 12394−12401.

22. Faller, P., Hasler, D. W., Zerbe, O., Klauser, S., Winge, D. R., and Vašák, M. (1999) Evidence for a dynamic structure of human neuronal growth inhibitory factor and for major rearrangements of its metal−thiolate clusters, *Biochemistry 38*, 10158−10167.
23. Roschitzki, B., and Vašák, M. (2003) Redox labile site in a Zn_4 cluster of Cu_4,Zn_4-metallothionein-3, *Biochemistry 42*, 9822−9828.
24. Vašák, M. (1991) Metal removal and substitution in vertebrate and invertebrate metallothioneins, *Methods Enzymol. 205*, 452−458.
25. Faller, P., and Vašák, M. (1997) Distinct metal−thiolate clusters in the N-terminal domain of neuronal growth inhibitory factor, *Biochemistry 36*, 13341−13348.
26. Weber, E., Jilling, T., and Kirk, K. L. (1996) Distinct functional properties of Rab3A and Rab3B in PC12 neuroendocrine cells, *J. Biol. Chem. 271*, 6963−6971.
27. Lanzetta, P. A., Alvarez, L. J., Reinach, P. S., and Candia, O. A. (1979) An improved assay for nanomole amounts of inorganic phosphate, *Anal. Biochem. 100*, 95−97.
28. Hunziker, P. E. (1991) Cysteine modification of metallothionein, *Methods Enzymol. 205*, 399−400.
29. Roschitzki, B., and Vašák, M. (2002) A distinct Cu_4-thiolate cluster of human metallothionein-3 is located in the N-terminal domain, *J. Biol. Inorg. Chem. 7*, 611−616.
30. Dumas, J. J., Zhu, Z., Connolly, J. L., and Lambright, D. G. (1999) Structural basis of activation and GTP hydrolysis in Rab proteins, *Structure 7*, 413−423.
31. Frederickson, C. J., Suh, S. W., Silva, D., Frederickson, C. J., and Thompson, R. B. (2000) Importance of zinc in the central nervous system: The zinc-containing neuron, *J. Nutr. 130*, 1471S−1483S.
32. Hasler, D. W., Faller, P., and Vašák, M. (1998) Metal−thiolate clusters in the C-terminal domain of human neuronal growth inhibitory factor (GIF), *Biochemistry 37*, 14966−14973.
33. Palumaa, P., Eriste, E., Njunkova, O., Pokras, L., Jornvall, H., and Sillard, R. (2002) Brain-specific metallothionein-3 has higher metal-binding capacity than ubiquitous metallothioneins and binds metals noncooperatively, *Biochemistry 41*, 6158−6163.
34. Romero-Isart, N., Jensen, L. T., Zerbe, O., Winge, D. R., and Vašák, M. (2002) Engineering of metallothionein-3 neuroinhibitory activity into the inactive isoform metallothionein-1, *J. Biol. Chem. 277*, 37023−37028.
35. Yamada, M., Hayashi, S., Hozumi, I., Inuzuka, T., Tsuji, S., and Takahashi, H. (1996) Subcellular localization of growth inhibitory factor in rat brain: Light and electron microscopic immunohistochemical studies, *Brain Res. 735*, 257−264.
36. Wang, X., Hu, B., Zimmermann, B., and Kilimann, M. W. (2001) Rim1 and rabphilin-3 bind Rab3-GTP by composite determinants partially related through N-terminal α-helix motifs, *J. Biol. Chem. 276*, 32480−32488.
37. Merithew, E., Stone, C., Eathiraj, S., and Lambright, D. G. (2003) Determinants of Rab5 interaction with the N terminus of early endosome antigen 1, *J. Biol. Chem. 278*, 8494−8500.
38. Pountney, D. L., Fundel, S. M., Faller, P., Birchler, N. E., Hunziker, P., and Vašák, M. (1994) Isolation, primary structures and metal binding properties of neuronal growth inhibitory factor (GIF) from bovine and equine brain, *FEBS Lett. 345*, 193−197.
39. Ostermeier, C., and Brunger, A. T. (1999) Structural basis of Rab effector specificity: Crystal structure of the small G protein Rab3A complexed with the effector domain of rabphilin-3A, *Cell 96*, 363−374.
40. Öz, G., Zangger, K., and Armitage, I. M. (2001) Three-dimensional structure and dynamics of a brain specific growth inhibitory factor: Metallothionein-3, *Biochemistry 40*, 11433−11441.
41. Biou, V., and Cherfils, J. (2004) Structural principles for the multispecificity of small GTP-binding proteins, *Biochemistry 43*, 6833−6840.
42. Chou, J. H., and Jahn, R. (2000) Binding of Rab3A to synaptic vesicles, *J. Biol. Chem. 275*, 9433−9440.
43. Rak, A., Pylypenko, O., Durek, T., Watzke, A., Kushnir, S., Brunsveld, L., Waldmann, H., Goody, R. S., and Alexandrov, K. (2003) Structure of Rab GDP-dissociation inhibitor in complex with prenylated YPT1 GTPase, *Science 302*, 646−650.
44. Zalewski, P. D., Millard, S. H., Forbes, I. J., Kapaniris, O., Slavotinek, A., Betts, W. H., Ward, A. D., Lincoln, S. F., and Mahadevan, I. (1994) Video image analysis of labile zinc in viable pancreatic islet cells using a specific fluorescent probe for zinc, *J. Histochem. Cytochem. 42*, 877−884.
45. Clifford, K. S., and MacDonald, M. J. (2000) Survey of mRNAs encoding zinc transporters and other metal complexing proteins in pancreatic islets of rats from birth to adulthood: Similar patterns in the Sprague-Dawley and Wistar BB strains, *Diabetes Res. Clin. Pract. 49*, 77−85.
46. Iezzi, M., Escher, G., Meda, P., Charollais, A., Baldini, G., Darchen, F., Wollheim, C. B., and Regazzi, R. (1999) Subcellular distribution and function of Rab3A, B, C, and D isoforms in insulin-secreting cells, *Mol. Endocrinol. 13*, 202−212.
47. Danscher, G., and Zimmer, J. (1978) An improved Timm sulphide silver method for light and electron microscopic localization of heavy metals in biological tissues, *Histochemistry 55*, 27−40.
48. Moffatt, P., and Seguin, C. (1998) Expression of the gene encoding metallothionein-3 in organs of the reproductive system, *DNA Cell Biol. 17*, 501−510.
49. Iida, H., Yoshinaga, Y., Tanaka, S., Toshimori, K., and Mori, T. (1999) Identification of Rab3A GTPase as an acrosome-associated small GTP-binding protein in rat sperm, *Dev. Biol. 211*, 144−155.
50. Guex, N., and Peitsch, M. C. (1997) SWISS-MODEL and the Swiss-PdbViewer: An environment for comparative protein modeling, *Electrophoresis 18*, 2714−2723.

BI047636D